Long-term (4 year) degradation behavior of coated stainless steel 441 used for solid oxide fuel cell interconnect applications

(article starts on next page)

Long-term (4 year) degradation behavior of coated stainless steel 441 used for solid oxide fuel cell interconnect applications

Claudia Goebel [a],[*], Robert Berger [b], Carlos Bernuy-Lopez [b], Jörgen Westlinder [b], Jan-Erik Svensson [a], Jan Froitzheim [a]

[a] Chalmers University of Technology, Department of Chemistry and Chemical Engineering, Division of Energy and Materials, Kemivägen 10, 41296, Gothenburg, Sweden
[b] Surface Research, Sandvik Materials Technology, Strategic Research, 81181, Sandviken, Sweden

HIGHLIGHTS

- Ce/Co coated (10/640 nm) AISI 441 is exposed for up to 38 000 h at 800 °C.
- Near parabolic mass gain behavior is found for the entire exposure length.
- Cr-evaporation rates after 37 000 h are similar to the initial rates.
- After 35 000 h at 800 °C the thermally grown oxide scale is roughly 15 μm thick.
- Even after 35 000 h of exposure low ASR values around 34 mΩcm^2 are measured.

ARTICLE INFO

ABSTRACT

The present work aims to investigate the long-term stability of Ce/Co coated AISI 441 used as an interconnect material in solid oxide fuel cells (SOFC). Being a commercially available alloy the use of AISI 441 would greatly reduce the cost of SOFCs in comparison to tailor-made interconnect materials such as Crofer 22 APU. To analyze the long-term stability Ce/Co coated AISI 441 is exposed in air at 800 °C for up to 38 000 h. Mass gain values are recorded continuously. After 7 000, 23 000, and 35 000 h area specific resistance (ASR) measurements are performed, and cross-sections are prepared and analyzed using scanning electron microscopy (SEM) and energy dispersive x-ray (EDX) spectroscopy. Cr-evaporation measurements are conducted on samples exposed for up to 38 000 h.

1. Introduction

Solid oxide fuel cells (SOFC) are a promising technology for green energy conversion systems, with many advantages, such as high electrical efficiency, scalability and fuel flexibility [1,2]. To achieve wide-spread commercialization of SOFCs, the key technical hurdles to overcome are their high cost and their limited life-time. Both factors can be influenced, amongst others, by improving the interconnect, an integral part of the SOFC, which connects individual cells to form a fuel cell stack and is typically made of a ferritic stainless steel [3]. Especially the transition from tailor-made interconnect materials, such as Crofer 22 APU and Sanergy HT, to a commercially available steel grade, such as AISI 441, can greatly decrease the overall cost of an SOFC [4]. However, the life-time of the interconnect is mainly limited by the corrosion of the steel due to high operating temperatures of the fuel cell, between 600 and 850 °C. These corrosion processes are known to be more severe for cheaper steel grades because these often have a lower Cr content [5–8]. Therefore, cheaper and commercially available steel grades could result in a decreased life-time compared to tailor-made steels. To avoid this, the use of highly protective coatings is necessary, especially for low cost steel grades. Today different coatings exist, and they differ not only in their effectiveness but also in what the coating influences. For example, some coatings mitigate Cr-evaporation, while others might reduce the oxide scale growth or lead to a more adherent oxide scale.

The most important material degradation mechanisms at 800 °C for interconnect materials are Cr-evaporation, which poisons the cathode, and the increase in electrical resistance, due to a continuously growing Cr$_2$O$_3$ scale [9].

To mitigate Cr-evaporation the most commonly used coatings today are spinel coatings, because they offer relatively high conductivities and they are fairly easy to deposit onto the steel [10–14]. Especially the (Co, Mn)$_3$O$_4$ (MCO) coating has gathered a lot of attention due to its promising Cr retention [15–17] and high electrical conductivity, σ = 60 S cm^{-1} for MnCo$_2$O$_4$ and σ = 6.4 S cm^{-1} for CoMn$_2$O$_4$ [18]. Besides applying this coating directly, via for example spray coating [19], screen printing [20], or electrophoretic deposition [21], the coating can also be applied via a conversion route [9,22–24]. For this, instead of applying the MCO coating directly to the steel, first a metallic Co coating is applied, for example, by using physical vapor deposition. At the operating temperature or sintering temperature of a SOFC this coating then oxidizes to form Co$_3$O$_4$ and subsequent outward diffusion of Mn from the steel leads to the formation of the desired MCO coating. Conversion coating routes are usually more cost effective than other coating techniques, as they can be applied in a large-scale roll-to-roll process, with subsequent shaping of the material to the final interconnect [25].

Another often used coating for interconnects is a reactive element coating. Reactive elements are elements that decrease the oxide scale growth and at the same time increase the oxide scale adherence [26,27]. In many tailor-made interconnect materials reactive elements have already been added to the alloy. However, this is not always the case for commercially available steels. For example, AISI 441 does not have any reactive elements as an alloying element. Therefore, to achieve the same effect, i.e. decreased oxide scale growth and increased oxide scale adherence, reactive element coatings are often applied [27,28]. The most commonly used reactive elements are Ce, La and Y. To be maximally effective these coatings have a lower and an upper thickness level, because too low reactive element concentrations will not result in any change in oxidation behavior, while too high reactive element concentrations can lead to an adverse effect [29].

Today one of the state-of-the-art coatings, that combines the effect of Cr-retention and decreased oxide scale growth is a Ce/Co coating with a 10 nm thick Ce layer beneath a 640 nm thick metallic Co layer [30,31].

Most studies on interconnect coatings are limited to exposure times around and below 1 000 h. However, for stationary applications lifetimes of at least 40 000 h are required, and so far, very little work has been done that focuses on the stability of the coating and the material for longer operation times [3,32]. *Linder* et al. [33] reported data on Sr-doped LaMnO$_3$ coated CFY that was run in a Galileo Hexis stack for 40 000 h at 900 °C. Similarly also *Groß-Barsnick* et al. [34] analyzed Mn$_{1.0}$Co$_{1.9}$Fe$_{0.1}$O$_4$ coated Crofer 22 APU interconnects that were operated in a stack for 34 000 h, but at 700 °C. Reactive element coatings on Crofer 22 APU were examined at 800 °C for up to 30 000 h by *Fontana* et al. [35] and the behavior of a Co conversion coating on different tailor-made steels was investigated by *Mikkelsen* et al. [36] at 750 °C for 10 000 h. Nevertheless, the long-term stability of an interconnect with regard to its mass gain behavior, its Cr retention and its electrical resistance needs to be further addressed, especially for the combination of a commercially available alloy such as AISI 441 and a highly effective coating such as Ce/Co. The present work analyzes these parameters for Ce/Co coated AISI 441 that was exposed in air for up to 38 000 h at 800 °C.

2. Materials and methods

2.1. Exposure

Two different batches of the ferritic stainless steel AISI 441 were used in this work. The composition of these can be found in Table 1. Unless stated otherwise all samples were Ce/Co coated with a 10 nm thick Ce layer beneath a 640 nm thick Co layer. The coatings were applied by Sandvik Materials Technology (SMT) using a proprietary Physical Vapor Deposition (PVD) technique. Prior to any exposures all samples were ultrasonically cleaned in acetone and in ethanol. All exposures were carried out at 800 °C. For long-term exposures (>3000 h) the sample size was 3 × 4 cm^2. These samples were exposed discontinuously in stagnant laboratory air in a box furnace at SMT and the mass gains were recorded continuously. After certain time intervals, 7 000 h, 23 000 h, 35 000 h, and 37 000 h samples were taken out of the furnace for further analysis (see Table 2). Exposures up to 3 000 h were carried out isothermally in tube furnaces at Chalmers. For these exposures an air flow of 6 000 sml min^{-1} and a humidity of 3% were employed. The sample size and the employed analytical methods varied for these short-term exposed samples and both can be found in Table 2. Further information on the analytical methods used in this work can be found in the following.

2.2. Cr-evaporation

For in-situ Cr-evaporation measurements a denuder technique developed by *Froitzheim* et al. [37] was employed. The measurements were carried out in tube furnaces at 800 °C with a predefined air flow of 6000 sml min^{-1} and a humidity of 3%. The samples that were exposed in box furnaces were too large for Cr-evaporation measurements, therefore, they were cut down to 3 × 2 cm using a low speed saw to limit the impact of the cutting process on the sample.

2.3. Area specific resistance

Area specific resistance (ASR) measurements were carried out on samples that were exposed in tube furnaces for up to 3 000 h and on samples that were exposed in box furnaces for up to 35 000 h. Prior to the ASR measurement a 1 cm^2 large Pt-electrode was applied to each sample. For this the area was first sputtered with a thin layer of Pt using the Quorom 150 sputter coater and, subsequently, painted with Pt paste, Metalor 6926. After drying and sintering the Pt paste for 10 min at 150 °C and 1 h at 800 °C, the ASR measurement was conducted in four-point probe DC mode using a NorECs Probostat in combination with a Keithley 2400 source meter. The current was set to 100 mA for all measurements

Table 2
Analysis on samples exposed at 800 °C for up to 37 000 h.

AISI 441 batch	Coating	Exposure	Exposure time (h)	Sample Size	Analysis technique
Batch A	Ce/Co	Discontinuous Box Furnace	37 000 + 1 200 h (Cr-evaporation)	3 × 4 cm	Cr-evaporation
Batch B	Ce/Co	Discontinuous Box Furnace	7 000 23 000 35 000	3 × 4 cm	ASR, BIB, SEM/EDX
Batch A	uncoated	Isothermal Tube Furnace	1 200 h	3 × 2 cm	Cr-evaporation ASR
Batch B	Ce/Co	Isothermal Tube Furnace	1 200 h	3 × 2 cm	Cr-evaporation ASR
Batch B	Ce/Co	Isothermal Tube Furnace	3 000 h	1.5 × 1.5 cm	ASR

Table 1
Composition of both AISI 441 batches in weight%.

AISI 441/EN 1.4509	Fe	Cr	Mn	Si	Ti	Nb	Ni	C	S	N
Batch 64313 (hereafter A)	Bal.	17.74	0.30	0.55	0.15	0.37	0.19	0.015	0.002	–
Batch 63960 (hereafter B)	Bal.	17.83	0.26	0.55	0.14	0.48	0.13	0.012	0.002	0.016

and besides measuring the ASR at the exposure temperature, it was also recorded during the cooling down period to verify semi-conducting behavior. Further information on this method can be found in Refs. [38,39].

2.4. Electron microscopy

After ASR measurements were conducted the microstructure of selected samples were analyzed using scanning electron microscopy (SEM) and energy dispersive x-ray (EDX) spectroscopy. First cross-sections were achieved using the broad ion beam (BIB) mill, Leica EM TIC 3X, then further analysis was performed using a Zeiss LEO Ultra 55 with an Oxford Inca EDX System.

3. Results

3.1. Gravimetric analysis

Fig. 1 shows the recorded mass gains for Ce/Co coated AISI 441 and uncoated AISI 441 which were exposed in air at 800 °C either discontinuously in a box furnace (BF) for up to 37 000 h or isothermally in a tube furnace (TF) for up to 3 000 h. Two different batches were used in the present study, because not enough material that had been exposed for longer than 3 000 h, was available from the same batch. The slight differences in compositions do not greatly impact the present study. This is verified by the mass gain behavior, which behaves similarly for both batches. Uncoated isothermally exposed AISI 441 showed a mass gain of around 0.3 mg cm^{-2} after 1 000 h of exposure. Longer exposures of uncoated materials were not conducted as this material is known to spall very quickly at temperatures above 800 °C if no coating is applied [9]. For all Ce/Co coated specimens an initial mass gain of around 0.21 mg cm^{-2} is visible due to the oxidation of the Co coating. A nearly parabolic mass gain behavior was found for long-term exposed Ce/Co coated AISI 441. Short-term and isothermally exposed samples ($\leq$ 3 000 h) showed similar mass gains after 1 000 h of exposure compared to discontinuously exposed samples. However, after 3 000 h isothermally exposed samples showed a slightly lower mass gain than discontinuously exposed
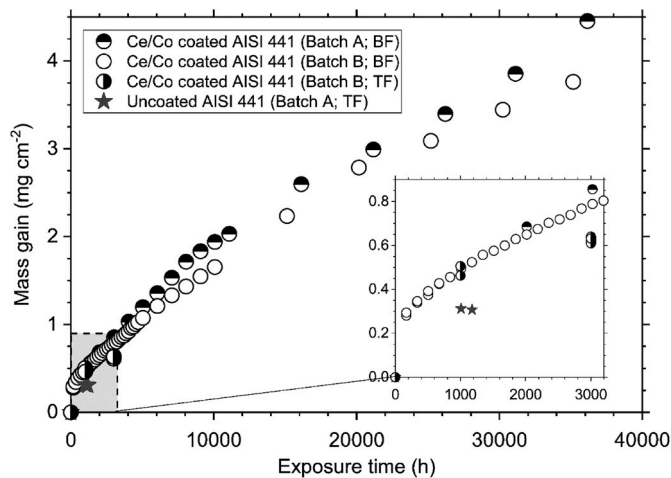
samples.

3.2. Cr-evaporation

Cr-evaporation measurements were conducted on unexposed and uncoated AISI 441, unexposed Ce/Co coated AISI 441 and 37 000 h exposed Ce/Co coated AISI 441. The results of these measurements can be found in Fig. 2. The average Cr-evaporation rate for uncoated AISI 441 was $1.8 \cdot 10^{-4}$ mg cm^{-2} h^{-1}. In comparison the Cr-evaporation rate for Ce/Co coated AISI 441 exposed for 1 000 h was reduced to $9.9 \cdot 10^{-6}$ mg cm^{-2} h^{-1}. The Cr evaporation for Ce/Co coated AISI 441 is still very low at the end of the 38 000 h of exposure, especially compared to uncoated AISI 441, with an average Cr-evaporation rate of $2.5 \cdot 10^{-5}$ mg cm^{-2} h^{-1}. The reason for the somewhat higher values after 37 000 h of exposure will be discussed below.

3.3. Area specific resistance

All recorded ASR values are depicted in Fig. 3a. Uncoated AISI 441 showed an average ASR value of around 33 mΩ cm^2 with a rather large spread after 1 000 h of exposure. On the other hand, the ASR values for all measured Ce/Co coated AISI 441 show comparatively little spread. The ASR values for the coated material also exhibited near parabolic behavior for the different exposure times. This is in agreement with the mass gain behavior. The average ASR value for Ce/Co coated AISI 441 was 20 mΩ cm^2 after 7 000 h, 32 mΩ cm^2 after 23 000 h, and 34 mΩ cm^2 after 35 000 h. Fig. 3b shows the Arrhenius plot for all measured Ce/Co coated AISI 441. Linear behavior was observed for all exposed samples. The slope of the orange line in the graph corresponds to the average slope of all measurements that were conducted on Ce/Co coated AISI 441. It corresponds to an activation energy of 0.51 eV.

3.4. Micro-structural investigation

SEM micrographs of BIB-cross-section for 0 h, 7 000 h, 23 000 h, and 35 000 h exposed Ce/Co coated AISI 441 are shown in Fig. 4. ASR measurements were conducted prior to the SEM analysis, except for the un-exposed sample; therefore, the Pt-electrode is visible in these micrographs. All phases were identified by EDX analysis and Fig. 5 depicts the EDX maps for 35 000 h exposed Ce/Co coated AISI 441.

The un-exposed material showed a rather flat interface between the steel and the coating. However, after 7 000 h of exposure especially the
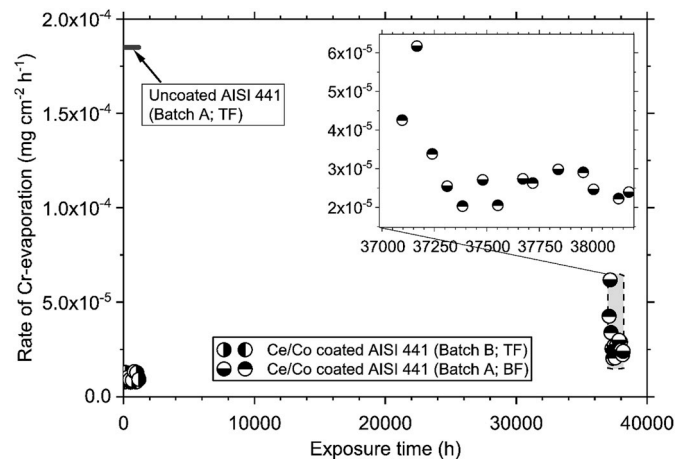

Fig. 1. Mass gain as a function of time for uncoated and Ce/Co coated AISI 441 exposed to air at 800 °C for up to 37 000 h. Different AISI 441 batches were used and are specified in brackets. Exposures were carried out discontinuously in box furnaces (BF) or isothermally in tube furnaces (TF). The mass gain values recorded for box-furnace exposed samples are average values over a range of samples, whereas all short-term ($\leq$ 3 000 h) exposed samples are specific values measured for one sample. The overall exposure time for Ce/Co coated AISI 441 batch A was 37 000 h. These samples were used for subsequent Cr-evaporation measurements. The overall exposure time for Ce/Co coated AISI 441 batch B was 35 000 h. These samples were used for subsequent ASR measurements.

Fig. 2. Cr-evaporation rate as a function of time for uncoated and Ce/Co coated AISI 441 exposed to air at 800 °C for up to 37 000 h. Different AISI 441 batches were used and are specified in brackets. Exposures were carried out discontinuously in box furnaces (BF) or isothermally in tube furnaces (TF). All Cr-evaporation measurements were carried out in tube furnaces. Rates for uncoated AISI 441 were averaged over the entire 1 000 h exposure.
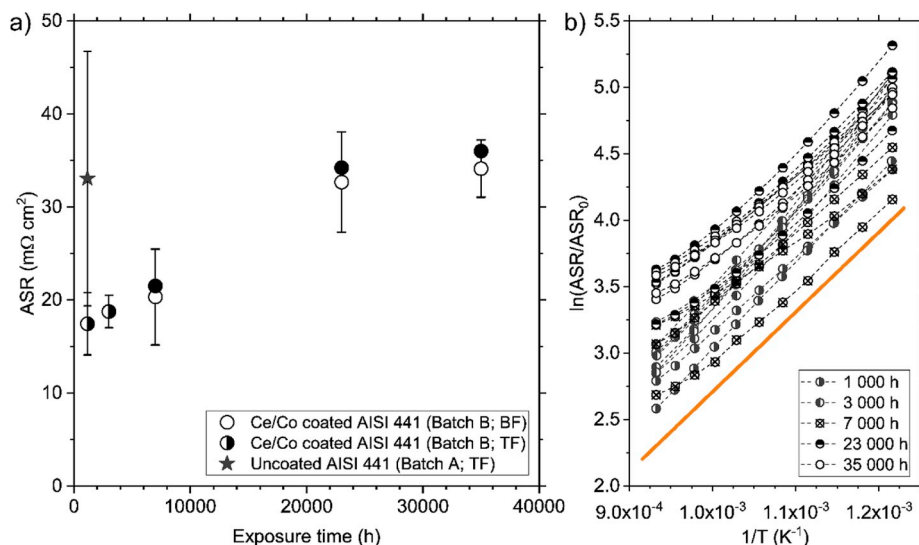
Fig. 3. a) Area specific resistance as a function of time for uncoated and Ce/Co coated AISI 441 exposed to air at 800 °C for up to 37 000 h. Different AISI 441 batches were used and are specified in brackets. Exposures were carried out discontinuously in box furnaces (BF) or isothermally in tube furnaces (TF). Empty symbols indicate average values with their respective standard deviation (error bars). Filled symbols indicate samples that were used for micro-structural analysis. b) Arrhenius plot for all Ce/Co coated AISI 441 samples. The slope of the orange line depicts the average activation energy.
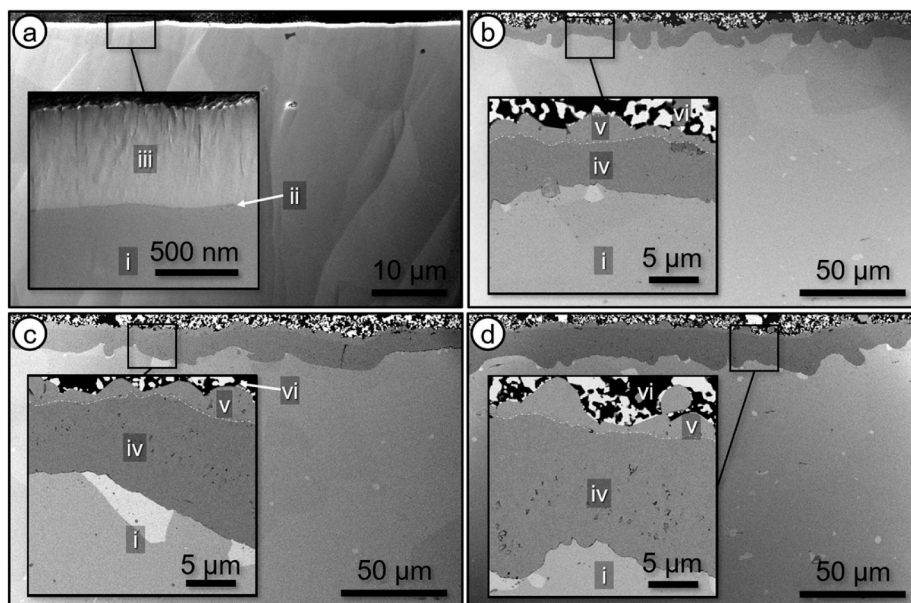

Fig. 4. Backscattered SEM micrographs for BIB milled cross-sections of Ce/Co coated AISI 441 exposed to air at 800 °C. Exposure lengths were a) 0 h, b) 7 000 h, c) 23 000 h and d) 35 000 h. Prior to preparing the cross-section, ASR values were measured for all exposed samples. The phases were identified as follows using EDX analysis: i) steel, ii) 10 nm Ce layer, iii) 640 nm Co layer, iv) Cr_2O_3, v) $(Co,Cr,Mn)_3O_4$, and vi) Pt-electrode.

interface between the steel and the oxide scale increases in roughness.

After exposure two distinct oxide layers are visible within the cross-sections, the $(Co,Cr,Mn)_3O_4$ spinel top layer and beneath it the thermally grown Cr_2O_3 layer. For the spinel layer the Co content ranges between 20 and 25 at% and the oxygen content stays constant at around 56 at%, however the Cr and Mn content vary significantly throughout the layer and between different samples. On the other hand, the thermally grown Cr_2O_3 layer showed a very high purity and density. The layer thickness for both layers and all exposure lengths are depicted in Table 3. Both oxide scales show a large variation in thickness, therefore the minimum and maximum values as well as the average and standard deviations for all layers are shown. The top spinel layer has roughly the same thickness for all exposure lengths.

Additionally, also the Cr content of the bulk material was determined using EDX point analysis. As mentioned above the original Cr content for this steel is around 17.8 wt%. This value is decreased to around 16.5 wt% after 7 000 h, 13.8 wt% after 23 000 h, and 11.8 wt% after 35 000 h of

exposure at 800 °C. The Nb and Si EDX maps also confirmed the presence of Laves phases within the alloy.

4. Discussion

After an initial fast increase, the mass gain behavior shows parabolic growth for Ce/Co coated AISI 441. Parabolic mass gain is present when the growth of the oxide scale, in this case Cr_2O_3, is diffusion-controlled by solid-state diffusion through the oxide scale. This process is described by the parabolic rate law formulated by Carl Wagner in 1933 [40]. Oxides that follow the parabolic rate law are often classified as protective, therefore the parabolic growth shown in the present work for Ce/Co coated AISI 441 indicates that protective behavior of the material is present even up to 37 000 h of exposure at 800 °C. The initial mass gain of 0.21 mg cm^{-2} for Ce/Co coated AISI 441 can be attributed to the oxidation of the metallic 640 nm thick Co coating and the ensuing formation of the Co_3O_4 as has been reported previously [9,31]. The
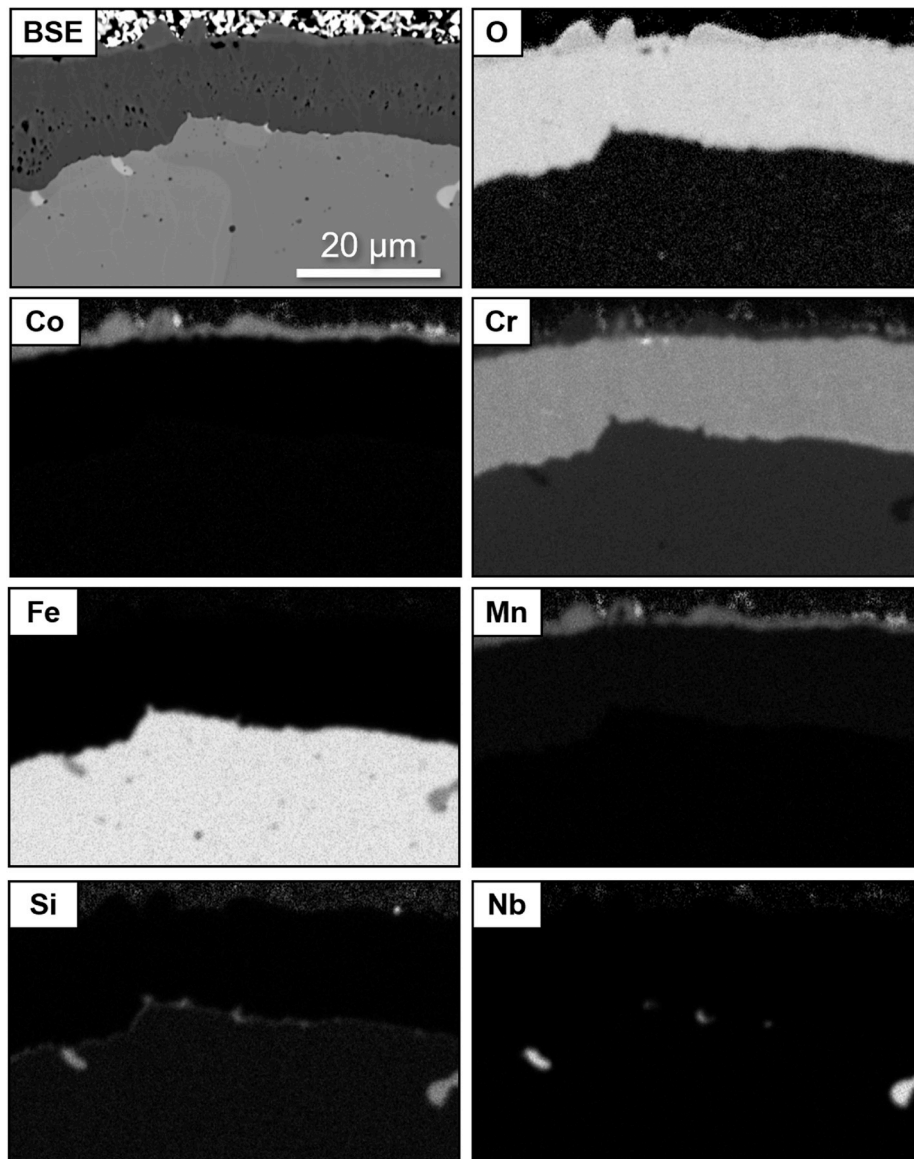
Fig. 5. Backscattered SEM micrograph and EDX maps for BIB milled cross-sections of Ce/Co coated AISI 441 that was exposed for 35 000 h at 800 °C in air. Prior to preparing the cross-section ASR values were measured. Ce maps were not included, as the Ce content was too low for the resolution of the SEM/EDX to detect it.

Table 3
Thickness for the $(Co,Cr,Mn)_3O_4$ spinel layer and the thermally grown Cr_2O_3 layer that formed on Ce/Co coated AISI 441, which was exposed for 7 000 h, 23 000 h, and 35 000 h in air at 800 °C. All values are given in μm.

Exposure Time	$(Co,Cr,Mn)_3O_4$ thickness (μm)				Cr_2O_3 thickness (μm)			
	Min	Max	Average	Standard Deviation	Min	Max	Average	Standard Deviation
7 000 h	1.5	2.6	2.0	0.6	4.5	9.8	6.5	1.9
23 000 h	0.7	3.4	2.2	1.1	7.0	15.6	10.9	3.0
35 000 h	2.7	3.1	2.9	0.2	10.9	18.1	14.9	2.8

difference between the mass gain of isothermally and discontinuously exposed samples after 3 000 h of exposure can be explained by the fact that the latter are repeatedly heated and cooled down again. Additionally, isothermally exposed samples were also subjected to a continuous humid air flow, this results in increased Cr-evaporation, which can in turn lead to a decrease in weight, and thus a decrease in mass gain.

The Ce/Co coating causes a reduction in Cr-evaporation rate by approximately one order of magnitude, similar to what has been reported previously [23]. Even though the coating is very thin (10/640 nm) no significant degradation of the coating can be found and the Cr evaporation rate is similar after 1 000 h and 38 000 h of exposure. The initially higher Cr-evaporation rate for 37 000 h exposed Ce/Co coated AISI 441 than for unexposed Ce/Co coated AISI 441 can be attributed to the preceding box furnace exposure. As mentioned earlier box furnace

exposures were carried out in stagnant laboratory air and the saturation of the furnace with Cr(VI) vapor species is expected to lead to an accumulation of Cr in the coating. During Cr-evaporation measurements in humid air and with a high air flow this accumulated Cr was then evaporated from the coating. This can be seen by the sharp decline of Cr evaporation rate for the data points between 37 000 and 37 200 h. Another factor that influences the Cr-evaporation rate of the pre-exposed Ce/Co coated AISI 441 is the unexposed and uncoated edge that is present for these samples, which resulted from having to cut the samples in half for the Cr-evaporation measurements. These factors can explain why the Cr-evaporation rate of pre-exposed Ce/Co coated AISI 441 is slightly elevated compared to the Cr-evaporation rate of the same material exposed for only 1 000 h.

In the present work very low ASR values were measured for Ce/Co coated AISI 441 specimens, further confirming that the coating is effective, not only in reducing the Cr-evaporation rate, but also in reducing the oxide scale growth even after 35 000 h. The values recorded after 3 000 h of exposure are in agreement with ASR values reported by *Magraso* et al. [41] for Ce/Co coated Sanergy HT exposed at 850 °C. Other previously published studies, however, reported higher ASR values for longer exposure times. For example, *Fontana* et al. [35] measured an ASR value of 73 mΩ cm^2 after 7 700 h of exposure at 800 °C for Y_2O_3 coated Crofer 22 APU, which increased to 160 mΩ cm^2 for 23 100 h of exposure. For the longer exposure times they observed a roughly 16 µm thick oxide scale, which was composed of a spinel oxide scale and a Cr_2O_3 scale. It is important to note that the spinel oxide formed in their work is a $(Mn,Cr)_3O_4$ spinel, which is significantly less electrically conductive than the $(Mn,Co)_3O_4$ spinel, which is formed in the present work. Furthermore the oxide scale in the present work is also significantly thinner after 23 000 h of exposure than the oxide scale that was reported by *Fontana* et al. [35].

The ASR values can also be calculated theoretically using the reported thickness values for the Cr_2O_3 scale (see Table 3) and literature data for the conductivity of Cr_2O_3. In our previous work [42] we have shown that the electrical resistance of the Co_3O_4 spinel is negligible for the overall resistance of the interconnect, because of the comparably poor conductivity of Cr_2O_3, $\sigma(Cr_2O_3) \leq 0.05$ S cm^{-1} [43–49], in comparison to the high electrical conductivity of Co_3O_4, $\sigma = 6.7$ S cm^{-1} [18]. This should be even more evident when a very thick Cr_2O_3 scale is present, as is the case after 35 000 h, therefore, for simplicity, the Co_3O_4 contribution was neglected in the calculation below.

To calculate the expected ASR value from the conductivity and the Cr_2O_3 scale thickness in Table 3 Equations (1) and (2) were used.

$$R = \frac{1}{\sigma} \cdot \frac{L}{A} \tag{1}$$

$$ASR = A \cdot R_{Cr_2O_3} = A \cdot \frac{1}{A} \cdot \frac{L_{Cr_2O_3}}{\sigma_{Cr_2O_3}} \tag{2}$$

where R is the resistance, σ is the conductivity, L is the thickness and A is the electrode area, which in the present work is A = 1 cm^2. The reported conductivity of Cr_2O_3 shows a large spread between different publications. This has been discussed elsewhere [38,42] but at 800 °C values range from 0.001 to 0.05 S cm^{-1} [43–49]. Because of this wide range of the conductivities, the ASR values were calculated for the highest and for the lowest reported conductivity. Additionally, theoretical ASR values were calculated for the minimum, maximum and average thickness values reported in Table 3 and for all three exposure lengths. The results can be found in Table 4.

For the highest σ values, reported by *Holt* et al. [45,50], the calculated ASR values match reasonably well with the measured ASR values. However, this is not the case for the lowest σ values, which were reported by *Crawford* et al. [43]. In general, the theoretical calculated ASR values show an immense spread and, therefore, they are perhaps not suitable to further evaluate the experimentally measured ASR values. Furthermore, in this work thermally grown oxides are present, which

Table 4
Average experimentally found ASR values (ASR$_{exp}$) for Ce/Co coated AISI 441, that was exposed in air at 800 °C and ASR values calculated (ASR$_{cal}$) from the thicknesses of the Cr_2O_3 layer reported in Table 3 and Equations (1) and (2).

Exposure Time (h)	ASR$_{exp}$ (mΩ cm^2)		L (µm)	$\sigma(Cr_2O_3)$ = 0.001 S cm^{-1} [43]	$\sigma(Cr_2O_3)$ = 0.05 S cm^{-1} [45,50]
				ASR$_{cal}$ (mΩ cm^2)	ASR$_{cal}$ (mΩ cm^2)
7 000	20	Min	4.5	452	9
		Max	9.8	977	20
		Average	6.5	650	13
23 000	32	Min	7.0	698	14
		Max	15.6	1562	31
		Average	10.9	1094	22
35 000	34	Min	10.9	1089	22
		Max	18.1	1814	36
		Average	14.9	1492	30

means that the incorporation of many different elements in the oxide scales is possible, which can influence the conductivity of the oxide scale. Additionally, the presence of an oxygen partial pressure gradient through the oxide scale can further alter the conductivity of the scale. Furthermore, the variation in thickness of the oxide scale can greatly impact the resistance, because it is expected that the thinnest parts of the oxide layer contributes most to the conductivity and thus the ASR values would be lower than expected from the mass gain data. Nevertheless, because of the good reproducibility of the ASR values over a large set of samples with relatively small error bars and the parabolic behavior of these values, the accuracy of the reported ASR measurements is high. Further verification of the ASR values reported in the present work is the behavior of all measured samples during cooling down. This behavior is reported in Fig. 3b. Because the resistance in the present case is dominated by Cr_2O_3, semi-conducting behavior should be expected of all measured samples.

Semi-conductors can be described by the Arrhenius equations, which is given in Equation (3).

$$ASR = ASR \cdot exp \frac{-E_a}{R \cdot T} \tag{3}$$

where E_a is the activation energy, R is the ideal gas constant and T is the absolute temperature. If semi-conducting behavior is present linear plots are expected when the natural logarithm is plotted as a function of T^{-1}. This is the case in the present work (see Fig. 3b). Furthermore, the resulting average activation energy in this work (slope of the linear plot) is 0.51 eV, which is well within the range of previously reported activation energies for Cr_2O_3, below 850 °C. For example, *Park* et al. [49] published an activation energy of 0.46 eV, *Crawford* et al. [43] reported a value of 0.51 eV and *Grolig* et al. [38] observed an activation energy of 0.52 eV. As discussed earlier the conductivity and therefore also the activation energy of Co_3O_4 should not greatly impact the overall conductivity behavior of the samples measured in the present work [42], thus the activation energy of Cr_2O_3 represents the semi-conducting behavior of all measured samples best.

All these results show that Ce/Co coated AISI 441 still exhibits protective behavior even after 38 000 h (37 000 h box furnace exposure + 1 000 h tube furnace exposure) of exposure in air at 800 °C. However, the bulk EDX measurements revealed that after 35 000 h of exposure, AISI 441 is quite depleted in Cr, with roughly 12 wt% Cr remaining in the steel. This indicates that material failure might occur soon. Nonetheless, even after 38 000 h no signs of breakaway corrosion were visible. To increase the longevity of this material further and to decrease the Cr consumption by decreasing the oxide scale growth rate, the amount of Ce could be increased [51]. This might result in a lower Cr depletion of the alloy after long exposure times.

5. Conclusion

In the present work it was shown that Ce/Co coated AISI 441 shows protective behavior at 800 °C even after 38 000 h of exposure. Besides having a parabolic mass gain behavior up to these long exposure times, it was also confirmed that the Cr-evaporation rates are still very low after 38 000 h, meaning that the Co coating has not yet failed. Even though a slight increase in Cr-evaporation rate compared to unexposed Ce/Co coated AISI 441 was observed for 37 000 h exposed Ce/Co coated AISI 441, this was attributed to the fact that one unexposed edge was present. Additionally, very low ASR values were found for 7 000 h, 23 000 h and 35 000 h exposed samples with an average ASR value of 34 mΩ cm^2 after 35 000 h. The SEM micrographs showed that a $(Co,Cr,Mn)_3O_4$ spinel had formed on top of a relatively pure Cr_2O_3 scale. The Cr_2O_3 scale grew in thickness over time and after 35 000 h the scale was in average 15 μm thick. Due to the very low Cr content of the bulk material after 35 000 h of exposure, material failure might be imminent. However, even after 38 000 h the material had not yet failed. To increase the life-time even further the Ce layer thickness could be increased. This could lead to a decreased Cr_2O_3 growth rate, which would delay the Cr depletion of the bulk.

Declaration of competing interest

The authors declare the following financial interests/personal relationships which may be considered as potential competing interests: The authors RB, CBL, and JW are employed at Sandvik Materials Technology. Sandvik Materials Technology manufactures Co/Ce coating under the trade name Sanergy HT 441. All experiments and characterization were carried out at Chalmers, except for the mass gain data presented in Fig. 1 (box furnace exposures).

Acknowledgments

References

[1] A.B. Stambouli, E. Traversa, Renew. Sustain. Energy Rev. 6 (2002) 433–455, https://doi.org/10.1016/S1364-0321(02)00014-X.

[2] M. Powell, K. Meinhardt, V. Sprenkle, L. Chick, G. McVay, J. Power Sources 205 (2012) 377–384, https://doi.org/10.1016/j.jpowsour.2012.01.098.

[3] J.W. Fergus, Mater. Sci. Eng., A 397 (2005) 271–283, https://doi.org/10.1016/j.msea.2005.02.047.

[4] P.D. Jablonski, C.J. Cowen, J.S. Sears, J. Power Sources 195 (2010) 813–820, https://doi.org/10.1016/j.jpowsour.2009.08.023.

[5] J. Fergus, Y. Zhao, ECS Trans. 35 (2011) 2447–2453, https://doi.org/10.1149/1.3570242.

[6] M.R. Ardigo, I. Popa, S. Chevalier, S. Weber, O. Heintz, M. Vilasi, Oxid. Metals 79 (2013) 495–505, https://doi.org/10.1007/s11085-012-9338-y.

[7] Z. Yang, G.-G. Xia, C.-M. Wang, Z. Nie, J. Templeton, J.W. Stevenson, P. Singh, J. Power Sources 183 (2008) 660–667, https://doi.org/10.1016/j.jpowsour.2008.05.037.

[8] W. Qu, L. Jian, D.G. Ivey, J.M. Hill, J. Power Sources 157 (2006) 335–350, https://doi.org/10.1016/j.jpowsour.2005.07.052.

[9] J.G. Grolig, J. Froitzheim, J.-E. Svensson, J. Power Sources 248 (2014) 1007–1013, https://doi.org/10.1016/j.jpowsour.2013.08.089.

[10] S. Geng, Y. Pan, G. Chen, F. Wang, Int. J. Hydrogen Energy 44 (2019) 9400–9407, https://doi.org/10.1016/j.ijhydene.2019.02.117.

[11] Q. Zhao, S. Geng, G. Chen, F. Wang, J. Alloy. Comp. 769 (2018) 120–129, https://doi.org/10.1016/j.jallcom.2018.07.333.

[12] C. Jia, Y. Wang, S. Molin, Y. Zhang, M. Chen, M. Han, J. Alloy. Comp. 787 (2019) 1327–1335, https://doi.org/10.1016/j.jallcom.2019.01.015.

[13] H. Ebrahimifar, Oxid. Metals 91 (2019) 417–435, https://doi.org/10.1007/s11085-019-09889-y.

[14] J. Li, C. Xiong, J. Li, D. Yan, J. Pu, B. Chi, L. Jian, Int. J. Hydrogen Energy 42 (2017) 16752–16759, https://doi.org/10.1016/j.ijhydene.2017.05.074.

[15] H. Kurokawa, C.P. Jacobson, L.C. DeJonghe, S.J. Visco, Solid State Ion. 178 (2007) 287–296, https://doi.org/10.1016/j.ssi.2006.12.010.

[16] R. Trebbels, T. Markus, L. Singheiser, J. Electrochem. Soc. 157 (2010) B490–B495, https://doi.org/10.1149/1.3298434.

[17] J. Froitzheim, J.E. Svensson, ECS Trans. 35 (2011) 2503–2508, https://doi.org/10.1149/1.3570248.

[18] A. Petric, H. Ling, J. Am. Ceram. Soc. 90 (2007) 1515–1520, https://doi.org/10.1111/j.1551-2916.2007.01522.x.

[19] Å.H. Persson, L. Mikkelsen, P.V. Hendriksen, M.A.J. Somers, J. Alloy. Comp. 521 (2012) 16–29, https://doi.org/10.1016/j.jallcom.2011.12.095.

[20] S.-I. Lee, J. Hong, H. Kim, J.-W. Son, J.-H. Lee, B.-K. Kim, H.-W. Lee, K.J. Yoon, J. Electrochem. Soc. 161 (2014) F1389–F1394, https://doi.org/10.1149/2.0541414jes.

[21] M. Mirzaei, A. Simchi, M.A. Faghihi-Sani, A. Yazdanyar, Ceram. Int. 42 (2016) 6648–6656, https://doi.org/10.1016/j.ceramint.2016.01.012.

[22] M. Stanislowski, J. Froitzheim, L. Niewolak, W.J. Quadakkers, K. Hilpert, T. Markus, L. Singheiser, J. Power Sources 164 (2007) 578–589, https://doi.org/10.1016/j.jpowsour.2006.08.013.

[23] J. Froitzheim, S. Canovic, M. Nikumaa, R. Sachitanand, L.G. Johansson, J.E. Svensson, J. Power Sources 220 (2012) 217–227, https://doi.org/10.1016/j.jpowsour.2012.06.092.

[24] X. Deng, P. Wei, M.R. Bateni, A. Petric, J. Power Sources 160 (2006) 1225–1229, https://doi.org/10.1016/j.jpowsour.2006.03.024.

[25] H. Falk-Windisch, M. Sattari, J.-E. Svensson, J. Froitzheim, J. Power Sources 297 (2015) 217–223, https://doi.org/10.1016/j.jpowsour.2015.07.085.

[26] N. Birks, G.H. Meier, F.S. Pettit, Introduction to the High-Temperature Oxidation of Metals, 2 ed., Cambridge University Press, Cambridge, 2006.

[27] P.Y. Hou, J. Stringer, Mater. Sci. Eng. A 202 (1995) 1–10, https://doi.org/10.1016/0921-5093(95)09798-8.

[28] K. Huang, P.Y. Hou, J.B. Goodenough, Mater. Res. Bull. 36 (2001) 81–95, https://doi.org/10.1016/S0025-5408(01)00506-2.

[29] J. Stringer, Mater. Sci. Eng. A 120–121 (1989) 129–137, https://doi.org/10.1016/0921-5093(89)90730-2.

[30] University of Birmingham, Scored 2:0 - Steel Coatings for Reducing Degradation, 2017. D 8.5.

[31] S. Canovic, J. Froitzheim, R. Sachitanand, M. Nikumaa, M. Halvarsson, L.G. Johansson, J.-E. Svensson, Surf. Coat. Technol. 215 (2013) 62–74, https://doi.org/10.1016/j.surfcoat.2012.08.096.

[32] N. Shaigan, W. Qu, D.G. Ivey, W. Chen, J. Power Sources 195 (2010) 1529–1542, https://doi.org/10.1016/j.jpowsour.2009.09.069.

[33] M. Linder, T. Hocker, L. Holzer, K.A. Friedrich, B. Iwanschitz, A. Mai, J.A. Schuler, J. Power Sources 243 (2013) 508–518, https://doi.org/10.1016/j.jpowsour.2013.05.200.

[34] S.M. Groß-Barsnick, Q. Fang, P. Batfalsky, L. Niewolak, L. Blum, W.J. Quadakkers, Fuel Cells 19 (2019) 84–95, https://doi.org/10.1002/fuce.201800050.

[35] S. Fontana, S. Chevalier, G. Caboche, Oxid. Metals 78 (2012) 307–328, https://doi.org/10.1007/s11085-012-9308-4.

[36] L. Mikkelsen, K. Neufeld, P.V. Hendriksen, ECS Trans 25 (2009) 1429–1436, https://doi.org/10.1149/1.3205675.

[37] J. Froitzheim, H. Ravash, E. Larsson, L.G. Johansson, J.-E. Svensson, J. Electrochem. Soc. 157 (2010) B1295, https://doi.org/10.1149/1.3462987.

[38] J.G. Grolig, Coated Ferritic Stainless Steels as Interconnects in Solid Oxide Fuel Cells, Doctor of Philosophy, Chalmers University of Technology, Gothenburg, Sweden, 2015, pp. 147–163.

[39] J.G. Grolig, J. Froitzheim, J.-E. Svensson, J. Power Sources 284 (2015) 321–327, https://doi.org/10.1016/j.jpowsour.2015.03.029.

[40] C. Wagner, Z. Phys. Chem. 21B (1933) 25, https://doi.org/10.1515/zpch-1933-2105.

[41] A. Magrasó, H. Falk-Windisch, J. Froitzheim, J.-E. Svensson, R. Haugsrud, Int. J. Hydrogen Energy 40 (2015) 8579–8585, https://doi.org/10.1016/j.ijhydene.2015.04.147.

[42] C. Goebel, A.G. Fefekos, J.-E. Svensson, J. Froitzheim, J. Power Sources 383 (2018) 110–114, https://doi.org/10.1016/j.jpowsour.2018.02.060.

[43] J.A. Crawford, R.W. Vest, J. Appl. Phys. 35 (1964) 2413–2418, https://doi.org/10.1063/1.1702871.

[44] W.C. Hagel, A.U. Seybolt, J. Electrochem. Soc. 108 (1961) 1146–1152, https://doi.org/10.1149/1.2427973.

[45] A. Holt, P. Kofstad, Solid State Ion. 69 (1994) 137–143, https://doi.org/10.1016/0167-2738(94)90402-2.

[46] P. Huczkowski, N. Christiansen, V. Shemet, L. Niewolak, J. Piron-Abellan, L. Singheiser, W.J. Quadakkers, Fuel Cells 6 (2006) 93–99, https://doi.org/10.1002/fuce.200500110.

[47] Y. Larring, R. Haugsrud, T. Norby, J. Electrochem. Soc. 150 (2003) B374–B379, https://doi.org/10.1149/1.1587726.

[48] H. Nagai, T. Fujikawa, K.-i. Shoji, Trans. Jpn Inst. Met. 24 (1983) 581–588, https://doi.org/10.2320/matertrans1960.24.581.

[49] J.H. Park, K. Natesan, Oxid. Metals 33 (1990) 31–54, https://doi.org/10.1007/BF00665668.

[50] A. Holt, P. Kofstad, Solid State Ion. 69 (1994) 127–136, https://doi.org/10.1016/0167-2738(94)90401-4.

[51] M.W. Lundberg, R. Berger, J. Westlinder, H. Holmberg, ECS Trans. 68 (2015) 1681–1689, https://doi.org/10.1149/06801.1681ecst.